Optical dipole traps for cold atoms using diffracted laser light

Glen D. Gillen* and Shekhar Guha
Air Force Research Laboratory, Materials and Manufacturing Directorate, Wright-Patterson Air Force Base, Dayton, Ohio 45433, USA

Katharina Christandl†
Department of Physics, The Ohio State University, Columbus, Ohio 43210, USA
(Received 30 June 2005; published 20 January 2006)

We theoretically investigate the feasibility of using intensity distributions of light of a single laser beam diffracted by a circular aperture as optical dipole traps for cold neutral atoms. Localized and cylindrically symmetric traps on the central axis of the circular aperture exist for both blue- and red-detuned laser light. Experimental mapping of the spots of interest using CO_2 laser light demonstrates the existence of these light distributions for laboratory conditions and their agreement with theoretical predictions.

DOI: 10.1103/PhysRevA.73.013409 PACS number(s): 32.80.Pj, 42.25.Fx

I. INTRODUCTION

Since the first theoretical prediction of trapping atoms using radiation pressure [1] and the first experimental observation of the optical dipole force on an atom [2] (both in 1978), a variety of approaches have been theorized and employed to trap atoms and particles using light. The first experimental observation of trapping dielectric particles using radiation pressure [3] (the method later known as "optical tweezers") was also reported simultaneously with the first experimental use of the optical dipole force to trap atoms [4] in 1986. Since then, a variety of approaches have been theorized and employed to trap atoms using the optical dipole force [5]. They include single-beam tight focusing for a single dipole trap [4], counterpropagating beams for one-dimensional lattices [6,7], two-dimensional [8,9], and three-dimensional lattices [9,10], and the focusing of Bessel light beams by axicons to create elongated traps and atom waveguides [11]. Recently, two-dimensional arrays of microlenses have been experimentally used for the creation of a two-dimensional array of atom traps using focused light [12]. In addition to methods employing focused and/or superimposed light beams, others have proposed the use of evanescent waves above a wave guide to trap atoms [13,14] and to create one and two-dimensional optical lattices [15].

In this paper we present the approach of using localized high and low intensity variations found in the near-field diffraction patterns of light incident upon a circular aperture for the trapping of cold neutral atoms using the dipole force. An advantage of this method over many currently employed approaches resides in the experimental simplicity of using a single unfocused (or loosely focused) laser beam incident upon a diffracting aperture. The method presented here is extendable to more complex diffraction masks consisting of a series of circular holes in one or two-dimensions and of varying diameters. Such diffraction masks would result in either one or two-dimensional arrays of dipole traps of varying dimensions, trap depths, and distances from the aperture plane.

II. VECTOR DIFFRACTION OF LASER LIGHT

Light distributions within and beyond a diffracting aperture can be accurately modeled using vector diffraction theory invoking the Hertz vector formalism [16,17], in which the polarization potential, or the Hertz vector $\mathbf{\Pi}$, of the light field incident upon the aperture is assumed to be known in the aperture plane.

The electric and magnetic fields for any point within the aperture plane and beyond can be calculated using a single vector potential function $\mathbf{\Pi}$:

$$\mathbf{E} = k^2\mathbf{\Pi} + \boldsymbol{\nabla}(\boldsymbol{\nabla}\cdot\mathbf{\Pi}) \tag{1}$$

and

$$\mathbf{H} = -\frac{k^2}{i\omega\mu_0}\boldsymbol{\nabla}\times\mathbf{\Pi} = ik\sqrt{\frac{\epsilon_o}{\mu_0}}\boldsymbol{\nabla}\times\mathbf{\Pi}, \tag{2}$$

where k is the wave number, ω is the angular frequency of the light, and μ_0 and ϵ_0 are the permeability and permittivity of free space, respectively. It has been assumed that the time dependence of the fields follows $e^{-i\omega t}$.

If the incident field is a uniform plane wave linearly polarized, say along the x axis, the electromagnetic field components at the point of interest can be calculated from the x component of the Hertz vector only [16], where

$$\Pi_x(x,y,z) = \frac{iE_0}{2\pi k}\int\int\frac{e^{-ik\rho}}{\rho}dx_0dy_0, \tag{3}$$

where E_0 is the electric field amplitude of the incident light and ρ is the distance from the integration point (x_0,y_0,z_0), in the aperture plane to the point of interest (x,y,z). The integration is performed over the open area of the aperture in the aperture plane. Once the Hertz vector has been calculated for

*Also at: Anteon Corporation, 5100 Springfield Pike, Dayton, Ohio, 45431; e-mail address: ggillen@anteon.com
†Currently at: Department of Physics, Kenyon College, Gambier, Ohio, 43022.

the point of interest, and **E** and **H** have been determined using Eqs. (1) and (2), the electromagnetic field intensity is given by the Poynting vector

$$\mathbf{S} = \mathrm{Re}(\mathbf{E} \times \mathbf{H}^*). \tag{4}$$

An important parameter in the diffraction of light by a circular aperture is the ratio of the radius of the aperture a to the wavelength of light λ. For aperture radius to wavelength ratios greater than 1, oscillations exist in the diffracted field intensity for points between the aperture plane and an axial distance of a^2/λ (see Ref. [17] for a more detailed discussion). In the aperture plane, the number of oscillations in the radial direction perpendicular to the polarization direction from the center of the aperture to the edge will be equal to a/λ, as will be the number of oscillations observed along the center axis of the aperture in the axial direction [17].

For distances larger than an aperture radius away from the aperture plane, calculations for the on-axis intensity distributions can be performed using the simpler Kirchhoff vector diffraction method [17]. Using Kirchhoff vector diffraction theory, an analytical expression for the on-axis electromagnetic fields can be derived. Due to symmetry, the transverse components of the Poynting vector are zero for points along the axis of the aperture, and the z component of the on-axis Poynting vector simplifies to

$$S_z(0,0,z) = S_0\left(\frac{1+2\left(\frac{z}{a}\right)^2}{1+\left(\frac{z}{a}\right)^2} - \frac{2\frac{z}{a}}{\sqrt{1+\left(\frac{z}{a}\right)^2}} \times \cos\left[kz\left(\sqrt{1+\left(\frac{a}{z}\right)^2}-1\right)\right]\right), \tag{5}$$

where $S_0 = \sqrt{\epsilon_0/\mu_0}|E_0|^2$ is the intensity of light incident upon the aperture.

From Eq. (5), the number and the axial locations $z(m)$ of the maxima and minima of $S_z(0,0,z)$ follow:

$$z(m) = \frac{a^2}{\lambda}\left(\frac{1}{m} - \frac{m\lambda^2}{4a^2}\right), \tag{6}$$

where m is an integer from 1 to $2a/\lambda$. Odd integer values of m correspond to on-axis intensity maxima, and even integer values correspond to on-axis minima; for example, $z(1)$ is the position of the on-axis maximum farthest from the aperture plane. For larger ratios of a/λ the farthest away on-axis maxima have relative intensities equal to approximately four times the light intensity incident upon the aperture, and the last few minima have absolute values very close to zero.

Figure 1 is an illustration using a color image plot of the calculated light field distributions of the z component of the Poynting vector versus the radial and axial positions (y and z) for 780-nm light incident upon a 25-μm diameter aperture and polarized in the x direction using the Hertz vector formalism, Eqs. (1)–(4). The colorized scale of Fig. 1 is normalized to the uniform light intensity incident upon the aperture. Beyond a distance of a^2/λ, or 200 μm, the beam profile has a single, central and radially symmetric maximum which smoothly expands in width and decreases in amplitude for larger and larger axial distances, similar to the behavior of a diverging laser beam. Between the aperture plane and distance of $z(m=1)$ an intricate diffraction pattern exists with localized regions of light and dark intensities. Figure 2 is a graph of the on-axis intensity of the diffracted laser light as a function of the distance from the aperture for the same axial range and parameters as in Fig. 1. Figure 2 illustrates the localization of high and low intensity levels along the central axis of beam propagation. The two points of interest of this paper are the on-axis positions of approximately 66 μm and 100 μm, or the locations of the second to last on-axis maximum and the last on-axis minimum. These localized intensity distributions correspond to possible optical dipole neutral atom traps for red and blue-detuned laser light, respectively.

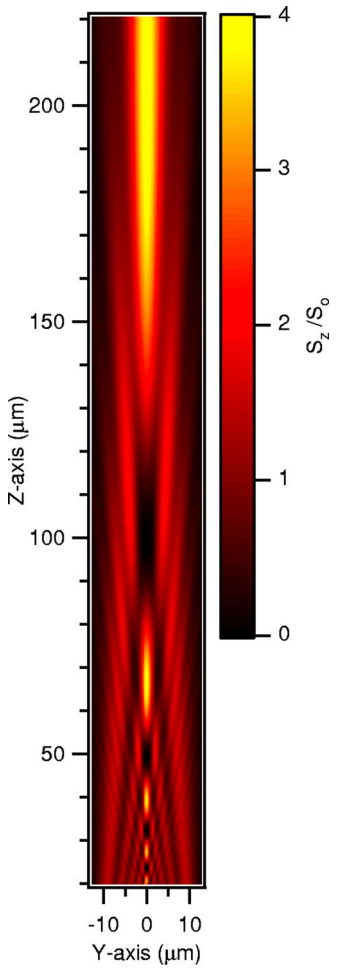

FIG. 1. (Color online) Calculated color image plot of the z component of the Poynting vector versus y and z for plane-wave, x-polarized, 780-nm light incident upon a 25-μm aperture. The relative intensity is normalized to the intensity incident upon the aperture.

Although numerous regions of localized high and low intensity light distributions exist closer to the aperture, only the two possible traps at locations of $z(m=2)$ and $z(m=3)$ are

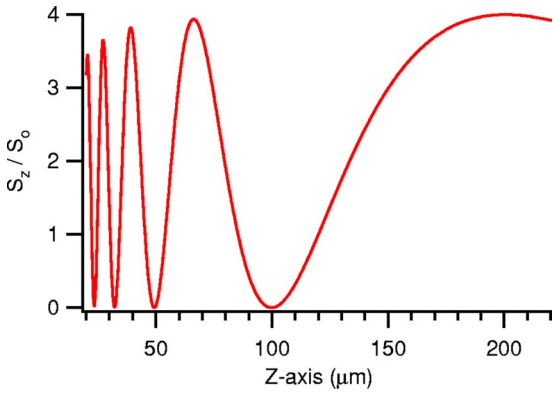

FIG. 2. (Color online) Calculated on-axis intensity of the z component of the Poynting vector versus the axial distance from the aperture plane for the same parameters as Fig. 1.

considered for further investigation in this work for three reasons. First, as the trap location approaches the aperture (higher m values) the theoretical traps become smaller, more tightly spaced and more tightly confined. Although these trap locations are theoretically appealing, these relative trap locations would present a higher level of difficulty to probe and address the trapped atoms experimentally. For example, the spacing between the on-axis blue-detuned traps of $m=10$ and $m=12$ is only 3.7 μm; whereas the spacing between the $m=2$ and $m=4$ traps are separated by 48 μm. Additionally, for m values greater than 4, the cross section of the intensity profiles indicate that there is a central ellipsoidal trap surrounded by one or more toroidal traps of comparable depths. The simplest experimental approach to address atoms trapped by diffracted laser light would be from an angle perpendicular to the axis of beam propagation. Thus, the toroidal traps surrounding the ellipsoidal traps would make addressing the central on-axis trap difficult. Finally, laboratory measurements of diffracted patterns show that significant deviations exist between theoretical intensity distributions and experimental light distributions as the axial distance approaches the aperture. Some of these intensity irregularities are illustrated and discussed further in Sec. IV for off-axis locations. For smaller axial distances, the measured discrepancies are attributed to experimental factors including: the deviation of the circularity of the aperture from that of a true circle, small deviations and irregularities of the incident laser beam profile from that of a uniform plane wave, and the deviation of the physical thickness of the aperture from that of an infinitely thin sheet.

III. SINGLE-BEAM OPTICAL DIPOLE TRAPS

An electric field **E** incident upon a polarizable particle will induce within the particle a dipole moment **p** and the interaction energy between the particle and the field is $-\mathbf{p}\cdot\mathbf{E}$. If the field is oscillating, and the particle's reaction to the field is in phase with the electric field, then the energy decreases with increasing field strength. If the induced dipole oscillation is exactly out of phase with the incident electric field, then the interaction energy is positive and the interaction energy of the particle increases with increasing field strength. For the case of a neutral alkali atom in a light field of frequency ω detuned from the resonant transition frequency ω_0 of the D2 transition ($^2S_{1/2} \rightarrow {}^2P_{3/2}$) the dipole interaction energy can be written as [13]

$$U(\mathbf{r}) = \frac{2}{3}\frac{\hbar\Gamma}{8}\frac{\Gamma}{\Delta}\left|\frac{E(\mathbf{r})}{E_s}\right|^2, \tag{7}$$

where Γ is the spontaneous emission decay constant, $\Delta=\omega-\omega_0$ is the detuning of the laser from the resonant frequency, $E(\mathbf{r})$ is the position-dependent electric field, and E_s is the saturation field of the optical transition. The sign of Δ determines whether or not the dipole interaction potential increases or decreases with respect to the gradient of the laser field. If the laser frequency is higher than the resonant frequency ("blue-detuned") then the interaction potential increases with an increasing laser field and the atoms are drawn towards low-field spots, or dark spots. If the laser frequency is "red-detuned" then the interaction potential drops with higher laser fields, and the atoms are drawn towards regions of higher field intensities.

As discussed in the previous section, the near-field distribution of light diffracted by a circular aperture contains numerous localized spots of alternating high and low laser intensities. For this work, two regions are of interest for optically trapping neutral atoms. One region is a strong candidate for the trapping of atoms using blue-detuned laser light, and the other is of interest for trapping atoms using red-detuned laser light. The primary spot of interest here for a blue-detuned trap (BDT) for trapping neutral atoms with blue-detuned laser light is the on-axis minimum farthest from the aperture (located at $z=100$ μm in Fig. 1). Using 780-nm laser light and a 25-μm diameter pinhole, the approximate size of this trap at full-width at half-maximum (FWHM) is roughly 5 by 50 μm, using the nearest intensity maxima in the radial and the axial directions. The primary spot of interest for this work for a red-detuned trap (RDT) for trapping atoms using red-detuned laser light is the second to last on-axis maximum observed in Fig. 1, located at $z=66$ μm. The approximate FWHM dimensions of this site are roughly 2.5 μm by 21 μm. Equation (5) can be used to evaluate the axial confinement of the traps. Unfortunately, analytical solutions to the diffracted intensity distributions can only be obtained for the special case of on-axis locations. Radial distributions must be numerically evaluated for each axial location of interest.

For cold ^{85}Rb atoms and 780-nm light, $\Gamma=2\pi\times 6$ MHz and $E_s=111.15V/m$, Eq. (7) can be written in a more convenient form as

$$\frac{U(\mathbf{r})}{S_0} = 9710\frac{\Gamma}{\Delta}\left(\frac{S_z(\mathbf{r})}{S_0}\right)\left(\frac{\mu\text{K cm}^2}{W}\right). \tag{8}$$

Equation (8) gives the position-dependent dipole trap potential in micro-K per unit intensity incident upon the aperture (in units of W/cm^2) for the normalized field intensity distributions (S_z/S_0) calculated in Figs. 1, 2, and 3(a). It is noted here that care must be taken in selection of the detuning and incident intensity parameters for red-detuned dipole traps

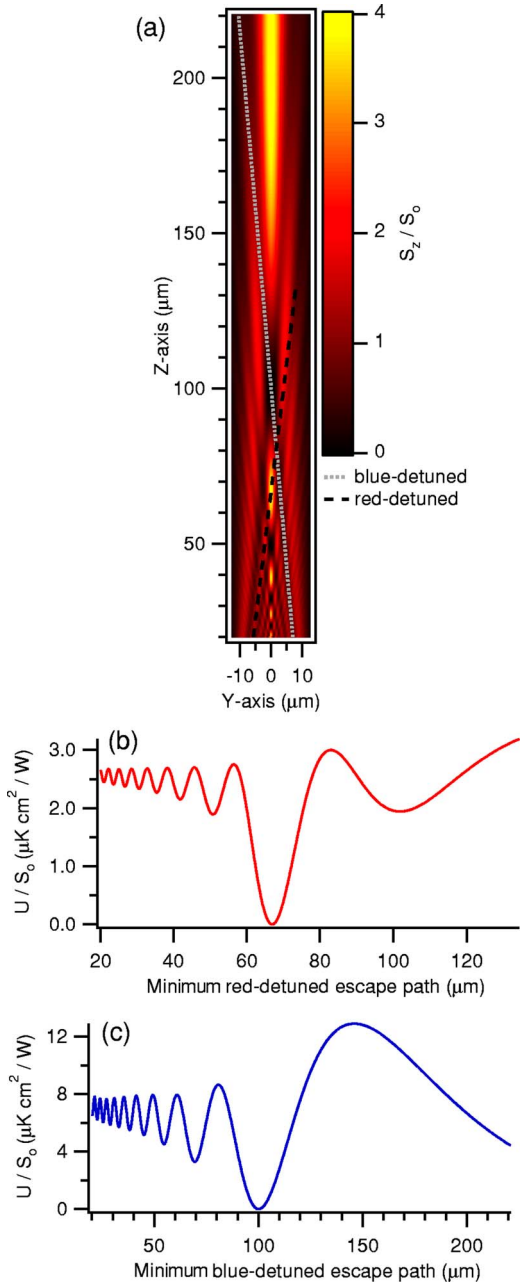

FIG. 3. (Color online) (a) Illustration of the minimum escape path from the on-axis dipole trap for red- and blue-detuned laser light. (b) and (c) are the dipole trap depths (in μK per W/cm^2 of laser intensity incident upon the aperture) for ^{85}Rb with $\Delta=-10^4\Gamma$ and $\Delta=10^3\Gamma$ versus position along the red- and blue-detuned minimum escape paths, respectively.

due to the fact that the dipole energy minimums occur at intensity maximums. Selection of appropriate parameters is necessary to avoid complications due to photon absorption, perturbation to the average potential from the excited state populations, trap heating, and the spontaneous force. In this investigation, we consider a detuning of $\Delta=10^3\Gamma$ for blue-detuned light, and $\Delta=-10^4\Gamma$ for red-detuned light.

Even by visual inspection of Fig. 1, it is evident that the minimum escape route for either a RDT or a BDT trapped atom is not going to be along the axis of beam propagation, or in the radial direction, but rather along a diagonal path over the lowest potential well wall. These minimum escape routes for a trapped atom to escape from either trap are illustrated in Fig. 3(a), and comprise a three-dimensional conical surface. Using Hertz vector diffraction theory, the position-dependent dipole interaction potential along the minimum escape cone for Rubidium atoms in red-detuned light ($\Delta=-10^4\Gamma$) is displayed in Fig. 3(b). Figure 3(c) is the position-dependent potential for blue-detuned light ($\Delta=+10^3\Gamma$) along a minimum escape path in the $x-z$ plane. The vertical scales of Figs. 3(b) and 3(c) have been converted into dipole trap depth in units of μK per W/cm^2 of uniform intensity incident upon the aperture using Eq. (8).

The RDT and BDT trap depths calculated and illustrated in Fig. 3 scale linearly with the intensity incident upon the aperture. Trap depths in the mK range are obtainable with sub-Watt level cw lasers. For example, if a 1 mK trap depth is desired, a BDT trap would require an incident intensity of 116 W/cm^2, and a RDT trap would require 364 W/cm^2. These incident intensities can be achieved if a 57 mW or a 178 mW cw laser beam is focused down to a Gaussian e^{-1} half width of 125 μm and incident upon the 25-μm diameter aperture, for BDT and RDT traps, respectively. The resulting radial f_r and axial f_z trap vibrational frequencies for a 1-mK BDT trap using 780-nm light and a 25-μm aperture would be $f_r=39$ kHz and $f_z=5.4$ kHz. The corresponding RDT trap frequencies would be $f_r=60$ kHz and $f_z=6.7$ kHz.

IV. EXPERIMENTAL MEASUREMENTS OF THE DIFFRACTED LIGHT BEAM

According to the theory presented in Sec. II (and that presented in Ref. [17]), the entire diffraction pattern generally scales as the ratio of a/λ. By scaling up the diffraction pattern calculated in Figs. 1 and 2 it is possible to experimentally probe and measure the intensity distributions around the possible red- and blue-detuned primary traps calculated in the previous section for 780-nm light, using conventional pinhole energy transmission scans. As a proof of principle, we describe here the experimental results obtained by using a longer laser wavelength, which allows for the use of a larger diffracting aperture, which in turn allows for a probe pinhole that is much smaller than the diffracting aperture, enabling detailed measurements of the diffraction patterns. The experimental setup chosen uses a CO_2 laser source tuned to a wavelength of 10.61 μm. The detector consists of a 5-μm pinhole, whose transmitted light is collected by a lens and refocused onto a liquid-nitrogen cooled HgCdTe detector. The aperture to wavelength ratio used for the calculations in Secs. II and III, is 15.4. Using 10.61-μm wavelength laser light, this ratio would correspond to an aperture diameter of 340 μm. A commercially available (Melles Griot) 400-μm pinhole was used for the diffracting aperture, resulting in a comparable aperture radius to wavelength ratio of 18.9. The laser used is a 2 W cw CO_2 laser by Access Laser Co. The beam incident upon the aperture is a TEM_{00} mode with a e^{-1} radius of 2 mm.

The entire detection assembly (5-μm pinhole, collection lens, and detector) is mounted on a computer controlled

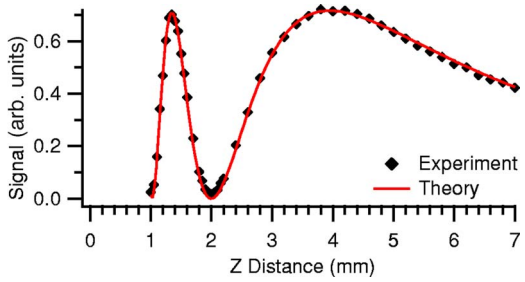

FIG. 4. (Color online) Experimental measured on-axis intensity distribution versus Hertz vector diffraction theory for $\lambda = 10.61$ μm and an aperture radius of 205 μm.

three-dimensional translation stage to enable a three-dimensional mapping of the diffracted light. In total, 51 high-resolution beam scans of the radial beam profile were collected at a variety of axial positions. Figure 4 is an illustration of the normalized central intensity of each beam scan as a function of the axial position of the detector pinhole with respect to the aperture plane, and compared to the theoretical on-axis intensity for an aperture to wavelength ratio of 18.9. The only slight deviation observed from the predicted on-axis intensity occurs through the last on-axis minimum, located approximately 2 mm from the aperture plane. This discrepancy was due to the noise floor of the detector's capability.

Figure 5 is a beam scan at an axial position of 1.33 mm, or the axial location of the possible primary red-detuned dipole trap. The scan covers an area of 250×250 μm with 100 points in each dimension. Near the center of the beam profile, the agreement is fairly consistent between the experimentally observed intensity and that predicted by theory, as seen in Fig. 5(a). Fluctuations and asymmetries in the radial profile are observed. These variations are believed to be due to variations in the circularity of the manufactured aperture, and deviations of the incident intensity of the laser from that of a true plane wave. Figure 6 is a similar illustration of the experimentally measured beam scan of the diffracted beam profile at a distance of 2 mm from the aperture, or the location of the possible primary blue-detuned dipole trap. As with the beam scan shown in Fig. 5, agreement between theoretical predictions and experimental measurement is fairly good near the center, with deviations occurring in the outer rings. Although experimental deviations and asymmetries were observed in the diffracted beam profiles away from the center of the beam, the predicted sharp and localized intensity maximum and minimum along the axis of propagation are in good agreement with theoretical predictions.

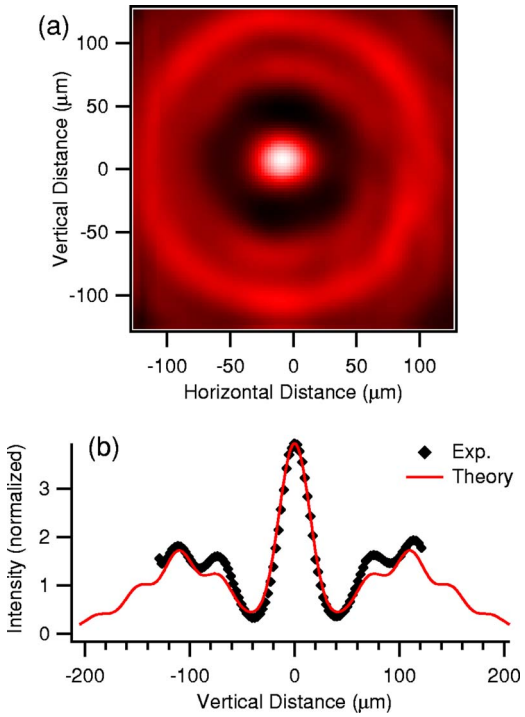

FIG. 5. (Color online) (a) Experimental scan of the beam profile for $\lambda = 10.61$ μm, $a = 205$ μm, $z = 1.33$ mm, and (b) the radial beam profile versus Hertz vector diffraction theory.

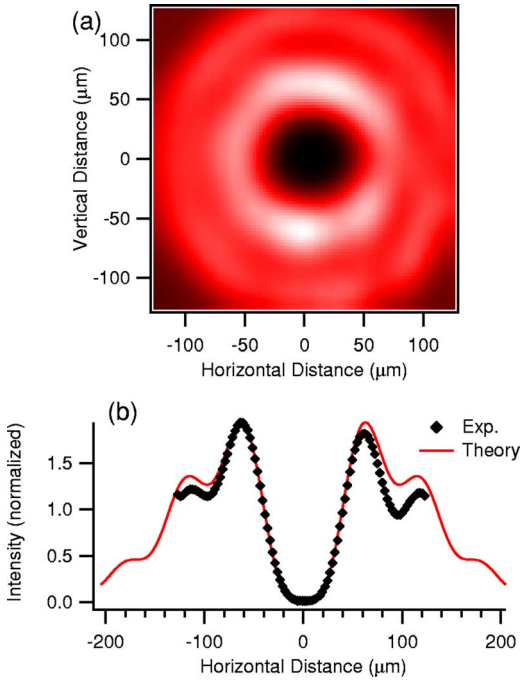

FIG. 6. (Color online) (a) Experimental scan of the beam profile for $\lambda = 10.61$ μm, $a = 205$ μm, $z = 2$ mm, and (b) the radial beam profile versus Hertz vector diffraction theory.

V. CONCLUSIONS

It has been previously shown [17] that near-field diffraction patterns can be accurately predicted using Hertz vector diffraction theory. Between the aperture plane and an axial distance of a^2/λ a series of sharp localized maxima and minima exist. The presence of these localized intensity variations, and the simplicity of a single beam setup make for an appealing alternative method to trap cold neutral atoms using diffraction patterns of laser light. Strong trap wells have been calculated for the trapping of neutral atoms using either blue

or red-detuned laser light. The potential spots for trapping neutral atoms with either blue or red-detuned laser light have been experimentally measured and observed for comparable aperture radius to wavelength ratios using infrared laser radiation. The method presented here is extendable to other diffraction masks of varying aperture sizes and arrays of apertures, yielding a variety of optical dipole trap sizes, depths, and arrays.

[1] A. Ashkin, Phys. Rev. Lett. **40**, 729 (1978).
[2] J. E. Bjorkholm, R. R. Freeman, A. Ashkin, and D. B. Pearson, Phys. Rev. Lett. **41**, 1361 (1978).
[3] A. Ashkin, J. M. Dziedzic, J. E. Bjorkholm, and S. Chu, Opt. Lett. **11**, 288 (1986).
[4] S. Chu, J. E. Bjorkholm, A. Ashkin, and A. Cable, Phys. Rev. Lett. **57**, 314 (1986).
[5] R. Grimm, M. Weidemüller, and Y. Ovchinnikov, Adv. At., Mol., Opt. Phys. **42**, 95 (2000).
[6] P. Verkerk, B. Lounis, C. Slomon, C. Cohen-Tanoudji, J.-Y Courtois, and G. Grynberg, Phys. Rev. Lett. **68**, 3861 (1992).
[7] D. L. Haycock, S. E. Hamann, G. Klose, and P. S. Jessen, Phys. Rev. A **55**, R3991 (1997).
[8] A. Hemmerich and T. W. Hänsch, Phys. Rev. Lett. **70**, 410 (1993).
[9] G. Grynberg, B. Lounis, P. Verkerk, J. -Y. Courtois, and C. Salomon, Phys. Rev. Lett. **70**, 2249 (1993).
[10] A. Hemmerich, C. Zimmermann, and T. W. Hänsch, Phys. Rev. Lett. **72**, 625 (1994).
[11] J. Arlt, K. Dholakia, J. Soneson, and E. M. Wright, Phys. Rev. A **63**, 063602 (2001).
[12] R. Dumke, M. Volk, T. Müther, F. B. J. Buchkremer, G. Birkl, and W. Ertmer, Phys. Rev. Lett. **89**, 097903 (2002).
[13] A. H. Barnett, S. P. Smith, M. Olshanii, K. S. Johnson, A. W. Adams and M. Prentiss, Phys. Rev. A **61**, 023608 (2000).
[14] J. P. Burke, S. T. Chu, G. W. Bryant, C. J. Williams, and P. S. Julienne, Phys. Rev. A **65**, 043411 (2002).
[15] K. Christandl, G. P. Lafyatis, S. C. Lee, and J. F. Lee, Phys. Rev. A **70**, 032302 (2004).
[16] G. Bekefi, J. Appl. Phys. **24**, 1123 (1953).
[17] S. Guha and G. D. Gillen, Opt. Express **13**, 1424 (2005).